https://doi.org/10.31436/iiumej.v26i2.4136

Optimal and Robust Speed Control of Electric Vehicles using a Hybrid Ant Colony Optimization Tuned Sliding Mode Control

PARTHIBAN S, KRISHNA S*

School of Mechanical Engineering, Vellore Institute of Technology, Vellore Campus, India

**Corresponding author: krishna.s@vit.ac.in*

(Received: 15 January 2026; Accepted: 16 March 2026; Published online: 10 May 2026)

ABSTRACT: Electric vehicle (EV) speed control is significantly affected by nonlinear motor dynamics, external disturbances, and parameter uncertainties, which degrade tracking performance and energy efficiency. Conventional controllers often fail to maintain robustness under varying operating conditions. Although Sliding Mode Control (SMC) provides strong robustness, it suffers from chattering and requires proper tuning of control parameters. To address this, a hybrid Ant Colony Optimization-based Sliding Mode Controller (ACO-SMC) is proposed to optimally tune the SMC control parameters. The performance of the ACO-SMC controller is evaluated using the US06 and FTP-75 driving cycles in MATLAB Simulink. The proposed controller outperforms the ACO-tuned proportional-integral-derivative (ACO-PID), conventional SMC, and PID controllers. The ACO-SMC controller significantly improves stabilization and robustness, even in the presence of measurement noise, external disturbance, and varying vehicle parameters. The results reveal that the hybrid ACO-SMC controller effectively minimizes chattering and maintains accurate speed control, even during sudden load disturbance and reference speed variations across all examined driving cycles. The integral absolute error (IAE) and integral squared error (ISE) are used as performance indices, achieving their minimum values over the complete US06 and FTP-75 driving cycles, thereby confirming the high accuracy of the proposed approach.

ABSTRAK: Kawalan kelajuan kenderaan elektrik (EV) dipengaruhi secara signifikan oleh dinamik motor tidak linear, gangguan luaran, serta ketidakpastian parameter, seterusnya menjejaskan prestasi penjejakan dan kecekapan tenaga. Pengawal konvensional lazimnya gagal mengekalkan keteguhan di bawah operasi yang berubah-ubah. Walaupun Kawalan Mod Luncur (SMC) menawarkan keteguhan yang tinggi, kaedah ini mengalami masalah *chattering* dan memerlukan penalaan parameter kawalan yang teliti. Bagi mengatasi isu ini, satu pengawal hibrid berasaskan Pengoptimuman Koloni Semut (ACO-SMC) dicadangkan bagi menala parameter SMC secara optimum. Prestasi pengawal ACO-SMC dinilai menggunakan kitaran pemanduan US06 dan FTP-75 pada MATLAB Simulink. Pengawal yang dicadangkan menunjukkan prestasi yang lebih baik berbanding pengawal PID yang ditala ACO (ACO-PID), SMC konvensional, dan PID biasa. ACO-SMC meningkatkan kestabilan dan keteguhan secara signifikan walaupun dalam kehadiran hingar pengukuran, gangguan luaran, serta variasi parameter kenderaan. Dapatan kajian menunjukkan bahawa pengawal hibrid ini berupaya meminimumkan fenomena *chattering* dan mengekalkan kawalan kelajuan yang tepat, termasuk semasa gangguan beban mendadak dan variasi rujukan kelajuan merentasi semua kitaran pemanduan yang diuji. Indeks prestasi seperti ralat mutlak berkamiran (IAE) dan ralat kuasa dua berkamiran (ISE) mencapai nilai minimum sepanjang satu kitaran penuh bagi kedua-dua kitaran pemanduan US06 dan FTP-75, sekaligus mengesahkan ketepatan tinggi melalui kaedah yang dicadangkan.

https://doi.org/10.31436/iiumej.v26i2.4136

KEYWORDS: *Sliding Mode Control (SMC), Ant Colony Optimization (ACO), EV speed control, MATLAB Simulink, Drive cycle*

1. INTRODUCTION

EVs are rapidly becoming the preferred option for sustainable and environmentally responsible transportation worldwide. The propulsion system plays a crucial role in determining the overall EV performance. Researchers from industry and academia have worked to improve control systems used in electric vehicle propulsion [1]. The controller should ensure low tracking error and minimal energy use. However, EV systems are highly nonlinear and time-varying, and are affected by changing road conditions, motor behavior, and external disturbances. This makes designing a controller that can handle disturbances and uncertainty while using low control effort challenging [2].

Traditional PID controllers are often used in industrial applications because they are simple and require minimal tuning [3]. But, they perform poorly under diverse operating conditions and do not guarantee the necessary dynamic performance [4]. Various methods have been proposed to fine-tune PID controllers, with the Ziegler–Nichols method being a widely recognized classical approach. This technique often provides good performance across many practical control systems [5]. However, in some cases, it fails, resulting in a significant overshoot in the system response.

Classical PI and PID controllers struggle under dynamic load conditions, prompting the development of adaptive control methods such as fuzzy logic (FL), adaptive Neuro-Fuzzy Inference System (ANFIS), Artificial Neural Network (ANN), and Sliding Mode Control (SMC). ANN controllers have gained attention for their effective performance in motor control applications, particularly for speed regulation and torque ripple reduction [6]. An optimization strategy was proposed in [7] to improve EV energy efficiency by reducing battery charging costs. Moreover, combining ANN techniques with traditional PID controllers yields significantly improved control performance, mainly due to the self-tuning capabilities of ANN algorithms [8]. However, ANN controllers face challenges, including large data requirements and long training times.

The fuzzy control method, based on fuzzy sets, linguistic rules, and decision-making theory, is an adaptive approach used in many applications [9]. Although fuzzy control has yielded successful results, correctly establishing the controller's rule base remains an important issue. SMC has become a highly effective technique for managing nonlinear systems due to its inherent robustness, strong stability, and ability to suppress external disturbances and parameter uncertainties. It is widely used in power electronics applications [10-11]. SMC ensures a rapid dynamic response by forcing the system's state trajectory to reach and stay on a predefined surface called the sliding surface. As a variable structure control method, it offers finite-time convergence and resilience to modeling inaccuracies, making it a reliable choice for modern control system design [12].

As noted in [13], the effectiveness of sliding mode control depends heavily on the selection of parameters that define the sliding surface. SMC involves two control signals: one during reaching mode and one in sliding mode. According to [14], switching control (u_{sw}) is employed during reaching mode to bring the system state onto the sliding surface, while the equivalent control (u_{eq}) in sliding mode ensures stable system behavior. A major drawback of this method is its discontinuous behavior, which causes high-frequency switching, or chattering, once the sliding surface is reached. This switching can excite unmodeled system

dynamics, leading to instability, degraded performance, or damage. Several approaches exist to reduce chattering. One common method is replacing the discontinuous switching function with a smooth, continuous one near the sliding surface. Another is high-order sliding mode control [15], which reduces chattering by controlling the higher-order derivatives of the sliding variable. These methods typically lower control gain as the system approaches the sliding surface, allowing the equivalent control to dominate once the surface is reached.

Alternative intelligent control methods, such as integrating SMC with fuzzy logic [16] or using Particle Swarm Optimization (PSO) [17], have been explored to enhance performance. However, these methods have limitations: fuzzy logic relies on heuristic rules with limited adaptability, and PSO and Genetic Algorithms (GAs) often suffer from premature convergence and require careful tuning. In contrast, Ant Colony Optimization (ACO) is a powerful metaheuristic that offers better global search, faster convergence, and adaptability to changing environments. These advantages make ACO more suitable for optimizing controller parameters in nonlinear and uncertain systems [18]. However, most existing ACO-SMC studies are limited to idealized step-reference tracking and do not adequately address realistic electric-vehicle operating conditions, including standard driving cycles and implementation constraints.

To address these limitations, this study presents an improved ACO-SMC-based speed control strategy for electric vehicles by integrating the optimization capability of ACO with the robustness of SMC, thereby achieving accurate, stable, and robust speed control across diverse driving conditions. Unlike existing studies that primarily focus on step reference inputs, the proposed controller is evaluated under standard electric vehicle driving cycles such as FTP-75 and US06, which represent practical vehicle operation. In addition, the controller's performance is quantitatively analyzed with respect to speed-tracking accuracy, disturbance-rejection capability, control-signal smoothness, chattering amplitude, and control RMS. Furthermore, system constraints such as control delay and voltage limitations are incorporated to ensure realistic performance evaluation. The main contributions of this work are summarized below:

- An optimized ACO-SMC controller is developed for electric vehicle speed control and validated under FTP-75 and US06 driving cycles.
- Comparative performance evaluation is conducted against SMC, PID, and ACO-PID controllers using ISE and IAE performance indices.
- Robustness of the proposed controller is verified through set-point tracking, external disturbance rejection, noise suppression, and sensitivity analysis.
- Chattering reduction and control signal smoothness are quantitatively analyzed using chattering amplitude and RMS value.

The rest of this paper is structured as follows: Section 2 covers the mathematical model of an electric vehicle. Section 3 outlines the proposed ACO-SMC hybrid controller framework for EV speed control. Section 4 presents the results and discussions. Section 5 summarizes the conclusions.

2. MATHEMATICAL MODEL OF ELECTRIC VEHICLE

The mathematical model of an EV is essential for analyzing its dynamic behavior and designing effective control strategies. The electric vehicle system primarily consists of a battery unit, a controller unit, and an electric motor that transmits power to the drivetrain. The dynamic behavior of the EV can be divided into two primary components: vehicle dynamics and motor

https://doi.org/10.31436/iiumej.v26i2.4136

dynamics. Despite PMSM and BLDC motors being widely used in modern EVs, DC motors remain suitable for low-power electric vehicles such as electric buggies and electric golf carts due to their simple dynamics and ease of control [18-21]. Therefore, a DC motor-driven electric vehicle is adopted in this work to validate the proposed ACO-SMC controller.

2.1. Vehicle Dynamics

Modeling the electric vehicle involves analyzing the balance of forces acting on the vehicle during motion. The key forces considered include rolling resistance (F_r), aerodynamic drag (F_{ad}), gravitational force (F_g), and the vehicle acceleration force (F_a) as illustrated in Figure 1. The total traction force (F_t) acts on the electric vehicle is expressed in Equation 2.

$$F_t = F_a + F_r + F_{ad} + F_g \tag{1}$$

$$F_t = ma + \mu_r mgcos\theta + 0.5\rho C_d A_f v^2 + mgsin\theta \tag{2}$$

Where m is the mass of the electric vehicle, a is the change in velocity over time, μ_r is the rolling resistance coefficient, g is the acceleration due to gravity, ρ is the air density, C_d is the drag coefficient, A_f is the vehicle frontal area, v is the vehicle velocity, θ is the slope angle.

The net force F_t acting on the vehicle generates a load torque T_L that is applied to the drive motor and can be expressed as,

$$T_L = F_t \times \frac{r}{G} \tag{3}$$

Where, G is the gearing ratio and r is the EV tire radius.

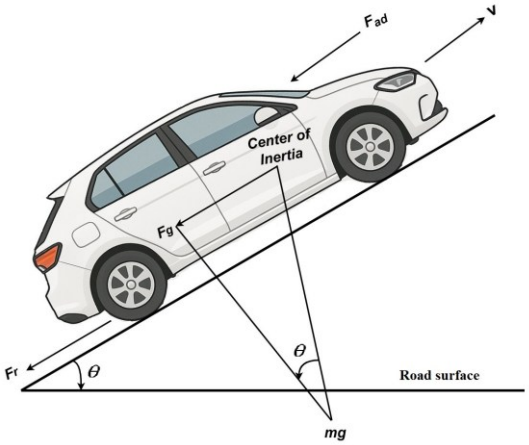

Figure 1. External forces acting on the EV

2.1. Motor dynamics

Considering a DC motor-driven electric vehicle, the motor dynamics can be modeled as,

$$\frac{d_i}{d_t} = \frac{V}{L_a+L_f} - \frac{(R_a+R_f)i}{L_a+L_f} - \frac{L_{af}i\omega}{La+L_f} \tag{4}$$

$$\frac{d\omega}{dt} = \frac{L_{af}i^2}{J} - \frac{B\omega}{J} - \frac{T_L}{J} \tag{5}$$

Where, ω is the motor angular speed, i is considered the field and armature current, L_f is the field winding inductance, L_a is the armature inductance, L_{af} is the mutual inductance, J is the motor moment of inertia, B is the viscous coefficient, V is the input voltage, T_L is the load torque, R_a is the armature resistance and R_f is the field winding resistance.

https://doi.org/10.31436/iiumej.v26i2.4136

The velocity to drive the vehicle is given by,

$$v = \omega \times \frac{r}{G} \tag{6}$$

The complete EV model, which combines both motor and vehicle dynamics, can be written as follows [20] and is implemented in Simulink, as illustrated in Figure 2. Table 1 describes the key parameters of the EV and the DC motor, along with their electrical specifications.

$$\frac{di}{d_t} = \frac{1}{(L_a + L_f)}\left[V - (R_{a+}R_f)i - i\omega L_{af}\right] \tag{7}$$

$$\frac{dw}{dt} = \frac{1}{\left[J+m\left(\frac{r}{G}\right)^2\right]}\left[L_{af}\, i^2 - B\omega - \frac{r}{G}\left(\mu_r mg + 0.5\rho A_f C_d v^2 + mg\, sin\theta\right)\right] \tag{8}$$

Equations 7 and 8 represent a nonlinear model that can be further converted into a state-space model.

$$\dot{x} = A(x) + B(x)\, u, y = C(x) \tag{9}$$

where

$$x = \begin{bmatrix} x_1 \\ x_2 \end{bmatrix} = \begin{bmatrix} i \\ \omega \end{bmatrix} \tag{10}$$

$$A(x) = \begin{bmatrix} -\dfrac{R_a + R_f}{L_a + L_f}\, x_1 - \dfrac{L_{af}}{L_a + L_f}\, x_1 x_2 \\ \dfrac{1}{J + m\left(\dfrac{r^2}{G^2}\right)}\left\{L_{af} {x_1}^2 - B x_2 - \dfrac{r}{G}\left(\mu_r mg + 0.5\rho A_f C_d \dfrac{r^2}{G^2}\, {x_2}^2 + mg\, sin\theta\right)\right\} \end{bmatrix}$$

$$B(x) = \begin{bmatrix} \dfrac{1}{L_a + L_f} \\ 0 \end{bmatrix}, C(x) = x_2$$

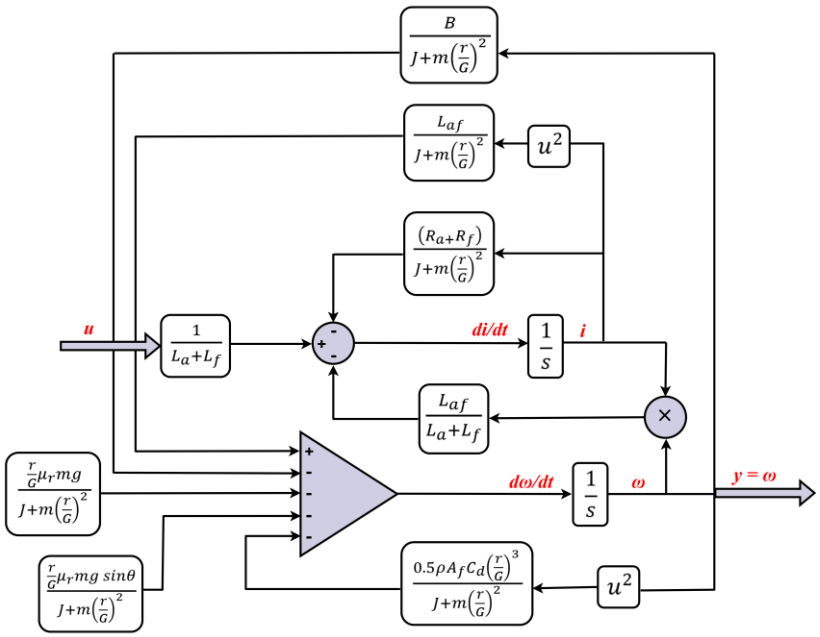

Figure 2. Overall structure of the EV system in Simulink

Table 1. EV specifications [20]

Parameters	Value	Parameters	Value
m	800 kg	$L_a + L_f$	6.00 mH
A_f	1.8 m^2	$R_a + R_f$	0.12 Ω
ρ	1.25 (kg/m^3)	J	0.05 kg m^2
C_d	0.3	L_{af}	1.76 mH
$c\theta$	0º	B	0.0002 N m s
G	11	i	78 A (250 max)
μ_r	0.015	V	48 V
r	0.25 m	ω	25 km/h

2.3. Inverter and Drive System Constraints

In practical electric vehicle systems, inverter efficiency, voltage limits, and control delays affect motor performance. In this study, these effects are considered by incorporating voltage saturation and system dynamics into the model. The control input voltage applied to the motor is limited using saturation bounds based on the rated motor voltage to ensure operation within the permissible range of the drive system. Additionally, the system dynamics inherently reflect the effects of inverter and actuator response delays. These constraints prevent the generation of unrealistic control signals and ensure safe motor operation. Thus, the simulation model provides a more realistic representation of the practical behavior of electric vehicle drive systems.

3. ACO-SMC Optimization Technique for EV Speed Improvement

The SMC controls the system's state trajectory toward a predefined sliding surface based on the system error, which is the deviation between the reference and the actual output. Once the system reaches this surface, it is forced to slide along it toward the equilibrium point. However, the conventional SMC controller suffers from excessive chattering and poor adaptability, which can directly affect the speed tracking performance and overall system stability. To overcome these challenges, this study uses an ACO-SMC-based controller that improves the system's adaptability and significantly reduces chattering. The proposed optimal SMC controller scheme for EV speed control is illustrated in Figure 3.

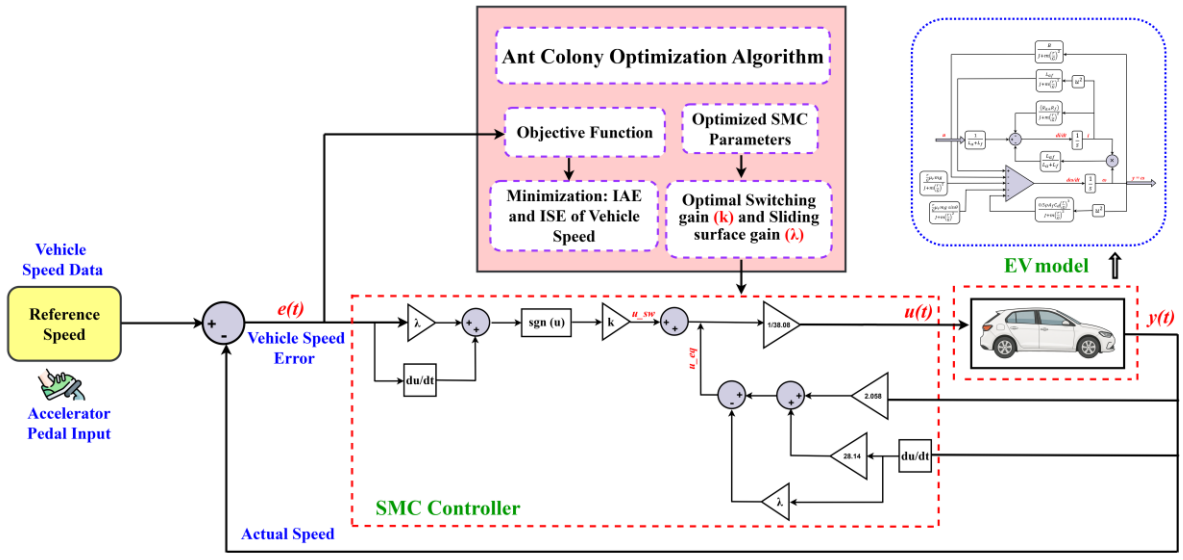

Figure 3. Proposed optimal SMC controller block diagram for EV speed control

https://doi.org/10.31436/iiumej.v26i2.4136

The control system integrates an ACO algorithm with the SMC to achieve robust and optimized EV speed regulation. The input is the reference speed from the driver's accelerator pedal, compared with the actual vehicle speed to generate the speed error e(t). This error signal is fed into the SMC controller, which computes the control signal $u(t)$ to operate the EV system. The performance of the SMC controller depends on the switching gain (K) and sliding surface gain (L). Instead of manual tuning, the ACO finds its optimal values by minimizing the IAE and ISE error metrics. Once these parameters are optimized, they are fed into the SMC controller to enhance speed accuracy and reduce chattering, ensuring adaptive EV speed control. The parameters of the ACO algorithm used for this study were selected based on standard recommended values from [18] and are listed in Table 2.

Table 2. ACO Parameters [18]

Parameters	Value
α	0.8
β	0.2
ρ	0.7
δ	0.01
No. of ants	30
No. of Iteration	30

The EV parameters in Table 1 are used in the simulation and controller design. The SMC controller is formulated using the state-space controllable form derived from Equation 9.

$$\ddot{\omega} + 28.14\dot{\omega} + 2.058\omega = 38.08v \tag{10}$$

Let us define the state variables as follows: $x_1 = \omega$, $x_2 = \dot{\omega}$ and take the control input as $u = v$. With these definitions, the system can be represented in state-space form using the controllable canonical structure:

$$\dot{x}_1 = x_2$$
$$\ddot{\omega} + 28.14\dot{\omega} + 2.058\omega = 38.08v \tag{11}$$

A sliding surface is then constructed by using the tracking error.

$$e(t) = \omega_{ref}(t) - \omega(t) \tag{12}$$

A first-order sliding surface is then formulated.

$$s(t) = \dot{e}(t) + Le(t)$$
$$s(t) = \dot{\omega}_{ref}(t) - \dot{\omega}(t) + L\left(\omega_{ref} - \omega\right) \tag{13}$$

where, ω_{ref} is the reference speed, ω is the actual speed, $e(t)$ is the error signal, and L is a positive sliding surface gain coefficient.

By using the Lyapunov function,

$$V(s) = \frac{1}{2}s^2 \tag{14}$$

To ensure system stability, the time derivative of the Lyapunov function presented in equation 14 must satisfy the condition $\dot{V}_{(s)} < 0$.

$$s\dot{s} < 0 \tag{15}$$

The derivative of the sliding mode function is

$$\dot{s} = \ddot{e} + L\ddot{e} \tag{16}$$

https://doi.org/10.31436/iiumej.v26i2.4136

$$\dot{s} = L\dot{e} + \ddot{\omega}_{r_{ef}} + 28.14\dot{\omega} + 2.058\omega - 38.08u \tag{17}$$

Thus, the derivative of the Lyapunov function $\dot{V}_{(s)}$ is

$$\dot{s}s = \left(L\dot{e} + \ddot{\omega}_{r_{ef}} + 28.14\dot{\omega} + 2.058\omega - 38.08u\right)s \tag{18}$$

To satisfy the condition $s\dot{s} < 0$, the control input is designed using the sliding mode control law given as,

$$u = \frac{1}{38.08}\left(2.058\omega + 28.14\dot{\omega} + \ddot{\omega}_{ref} + L\dot{e} + K\,sgn(s)\right) \tag{19}$$

The sliding mode controller was modified to reduce the chattering effect, as

$$u = \frac{1}{38.08}\left(2.058\omega + 28.14\dot{\omega} + \ddot{\omega}_{ref} + L\dot{e} + K\,\frac{s}{|s|+\delta}\right) \tag{20}$$

Where,

$$sign(s) = \begin{bmatrix} 1 & if\ s > 0 \\ 0 & if\ s = 0 \\ -1 & if\ s < 0 \end{bmatrix} \tag{21}$$

δ is the scalar tuning parameter to reduce the chattering effect, and K is the switching gain coefficient.

Substitute (20) for (15), then we get,

$$s\dot{s} = -k\,sgn(s) < 0 \tag{22}$$

ACO is a robust and adaptive metaheuristic algorithm inspired by the foraging behavior of real ant colonies. Ants communicate indirectly through pheromone deposition, allowing them to find optimal paths or solutions over time. In this algorithm, artificial ants explore possible paths from an initial state to a target solution, guided by a combination of pheromone trails and heuristic information. The process is iterative, and paths associated with better solutions receive higher pheromone deposits, making them more attractive to subsequent ants. The pheromone matrix, written as $\tau = \{\tau_{ij}\}$ is used to find the optimal solution. The initial state of the pheromone matrix is given by,

$$\tau_{ij} = \tau_0\,\psi_{(i,j)} \tag{23}$$

where, $\tau_0 > 0$. The probability $\{P_{ij}^A\}$ of selecting a node i at node j is given as

$$P_{ij}^A = \frac{[\tau_{ij}]^{\alpha}\cdot[\eta_{ij}]^{\beta}}{\Sigma_{(i,j)\in T^A}[\tau_{ij}(t)]^{\alpha}\cdot[\eta_{ij}]^{\beta}} \tag{24}$$

where T^A represents the path followed by an ant A at a given time, α and β are indeed constants that control the impact of pheromone values and the influence of the heuristic value on an ant's decision. The heuristic factor η_{ij} is given by

$$\eta_{ij} = \frac{1}{d_{ij}}, i = [L, K] \tag{25}$$

where d_{ij} is the distance between nodes i and j.

Using the SMC control law in equation 20, the parameters K and L are evaluated using the heuristic factor in equation 25. The quality of the pheromones $\Delta{\tau_{ij}}^A$ at each path is defined as

https://doi.org/10.31436/iiumej.v26i2.4136

$$\Delta\tau_{ij}{}^{A} = \begin{bmatrix} \frac{L^{min}}{L^{A}} \\ 0 \end{bmatrix} \quad (26)$$

where, L^A is the objective function value found by the ant A and L^{min} is the best solution carried out by the set of ants A until the current iteration.

The pheromone updating is,

$$\sum_k \Delta\tau^k = \Delta_\tau^{k=1} = \frac{\zeta f_b}{f_w} \quad (27)$$

Pheromone evaporation plays a crucial role in preventing the excessive accumulation of pheromone trails,

$$\tau_{ij}(t) = (1-\rho)\tau_{ij}(t-1) + \sum_{A=1}^{NA} \Delta\tau_{ij}^{A}(t) \quad (28)$$

where NA is the number of ants, while ρ is the evaporation rate.

A controller is considered optimal when its control parameters are tuned to minimize a predefined cost function. The objective function (K, L) is formulated to minimize the integral absolute error (IAE) and integral squared error (ISE) between the reference and the actual speed over a specified time duration.

$$\text{IAE} = \int_0^\infty |\text{e}(t)|\, \text{d}t \quad (29)$$

$$\text{ISE} = \int_0^\infty e^2(t)\, \text{d}t \quad (30)$$

4. Results and Discussion

The proposed ACO-SMC controller minimizes the objective functions defined in equations 29 and 30 to obtain the optimal control parameters for the SMC controller. To evaluate the controller's performance under realistic conditions, the FTP-75 and US06 driving cycles are used as reference speed profiles. The controller is tested under four main scenarios: set-point tracking, noise suppression, disturbance rejection, and sensitivity analysis to examine robustness, accuracy, and effectiveness.

4.1. Evaluating ACO-SMC for FTP-75 and US06 driving cycles

To evaluate the performance of the proposed ACO-SMC controller for an EV, the FTP-75 (cold stabilization phase) and US06 driving cycle were used as the reference speed profiles to represent urban and highway driving conditions, respectively. The SMC controller calculates the tracking error $e(t)$ as the difference between the reference speed and the actual speed. Initially, the sliding surface gain L = 5 and switching gain K = 10 for FTP-75, L = 5 and K = 10 for US06 were assigned for controller tuning. Afterward, they are tuned using the ACO algorithm for 30 iterations, yielding optimized gain values of L = 9.809 and K = 16.426 for FTP-75, and L = 9.096 and K = 29.42 for US06, based on the evaluation of performance metrics IAE and ISE.

4.1.1. Set-point tracking

The set-point tracking performance of PID, conventional SMC, ACO-PID, and the proposed ACO-SMC controllers was evaluated under both FTP-75 and US06 driving cycles. During the FTP-75 cycle, the PID, SMC, and ACO-PID controllers exhibit noticeable tracking errors, particularly during rapid speed transitions between 460 s and 510 s. In contrast, the

https://doi.org/10.31436/iiumej.v26i2.4136

proposed ACO-SMC controller closely follows the reference speed with minimal tracking error, as shown in Figures 4a and 4b. Similarly, under the aggressive US06 driving cycle, the proposed controller maintains superior tracking performance despite rapid speed variations between 146 and 186 seconds, as shown in Figures 5a and 5b. The control signal comparison is shown in Figures 6a and 6b for FTP-75 and US06, respectively. It is observed that the PID and conventional SMC controllers produce high-frequency oscillations and larger control variations due to poor tuning and chattering effects. The ACO-PID controller reduces these oscillations to some extent, whereas the proposed ACO-SMC controller produces the smoothest control signal with minimal oscillations.

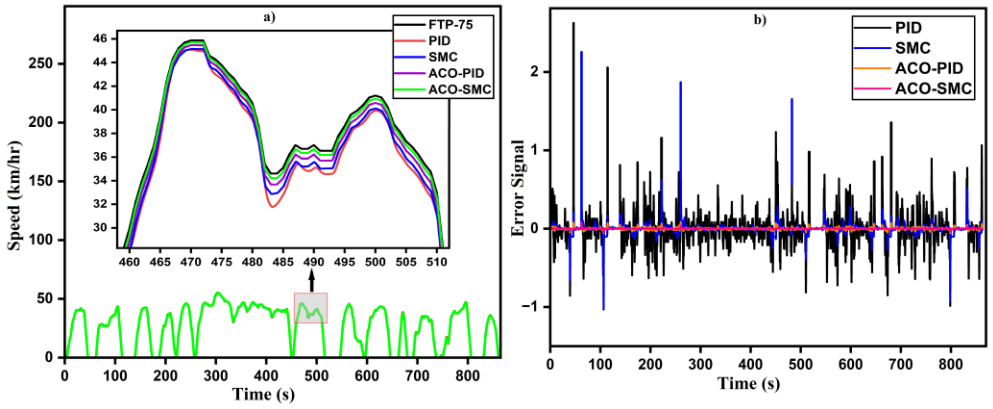

Figure 4. a) FTP-75 Speed tracking, b) FTP-75 Error analysis

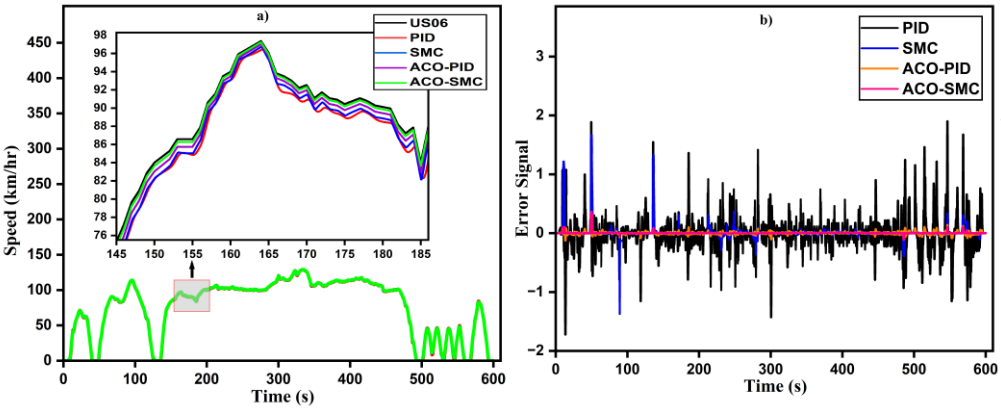

Figure 5. a) US06 Speed tracking, b) US06 Error analysis

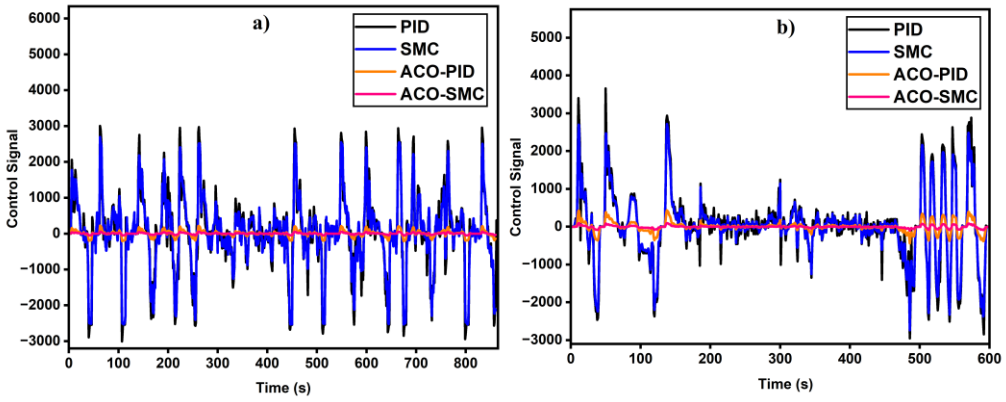

Figure 6. a) FTP-75 Control effort, b) US06 Control effort

Table 3. Performance metrics for FTP-75 and US06

	Performance Metrics	IAE	ISE	Control RMS	Chattering Amplitude
FTP-75	PID	10.03	1.594	2.85	1.92
	SMC	6.329	0.762	2.21	1.35
	ACO-PID	2.521	0.071	1.74	0.82
	ACO-SMC	1.525	0.029	1.12	0.38
US06	PID	12.26	2.135	3.94	2.85
	SMC	9.01	1.806	2.95	1.96
	ACO-PID	4.88	0.422	2.18	1.21
	ACO-SMC	3.25	0.152	1.48	0.62

Table 3 summarizes the performance metrics for the FTP-75 and US06 cycles. The proposed ACO-SMC controller achieves the lowest IAE and ISE values for both cycles, indicating improved tracking accuracy. Furthermore, the ACO-SMC control RMS and chattering amplitude values are significantly lower than those of PID, SMC, and ACO-PID, indicating smoother and more efficient control. Overall, the proposed ACO-SMC controller provides superior tracking performance, smoother control signal, and reduced chattering under both FTP-75 and US06 driving cycles.

4.1.2. Noise suppression

To evaluate the robustness of the ACO-SMC controller, measurement noise was introduced into the speed feedback signal to represent realistic sensor inaccuracies, with an amplitude range of -0.05 to +0.05 and a sampling time of 0.01 seconds. As shown in Figure 7, the PID, conventional SMC, and ACO-PID controllers exhibit noticeable speed fluctuations under noisy conditions. In contrast, the proposed ACO-SMC controller effectively suppresses noise-induced oscillations by maintaining a smoother, more stable speed response, demonstrating superior noise rejection.

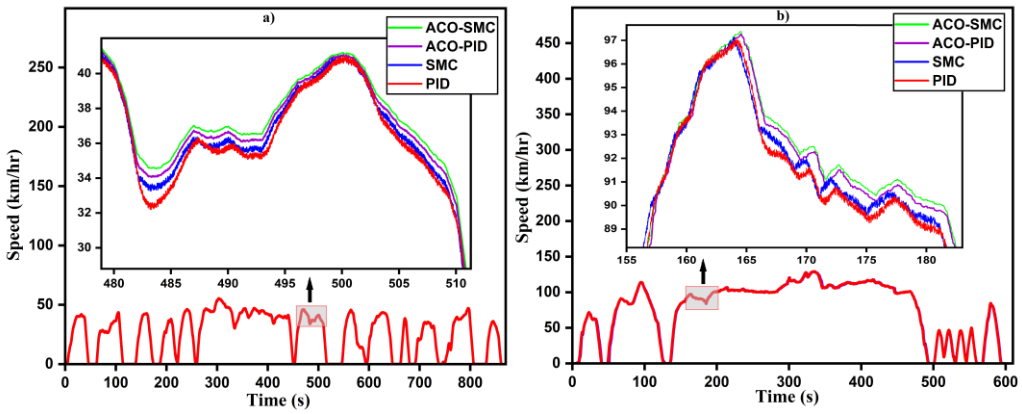

Figure 7. Performance of the controller in the presence of measurement noise for FTP-75 and US06

4.1.3. External disturbance rejection

To evaluate the effectiveness of the ACO-SMC controller, an external disturbance was introduced into the system as a step signal of 1km/h, representing a static disturbance at t = 303 s for the FTP-75 and t = 163 s for the US06 cycle, respectively. As shown in Figure 8, the PID, conventional SMC, and ACO-PID controllers exhibit noticeable deviations from the reference speed due to the external disturbance. In contrast, the proposed ACO-SMC controller effectively restores the vehicle speed to the reference speed with a shorter recovery time,

demonstrating superior robustness against external disturbances and better speed regulation performance.

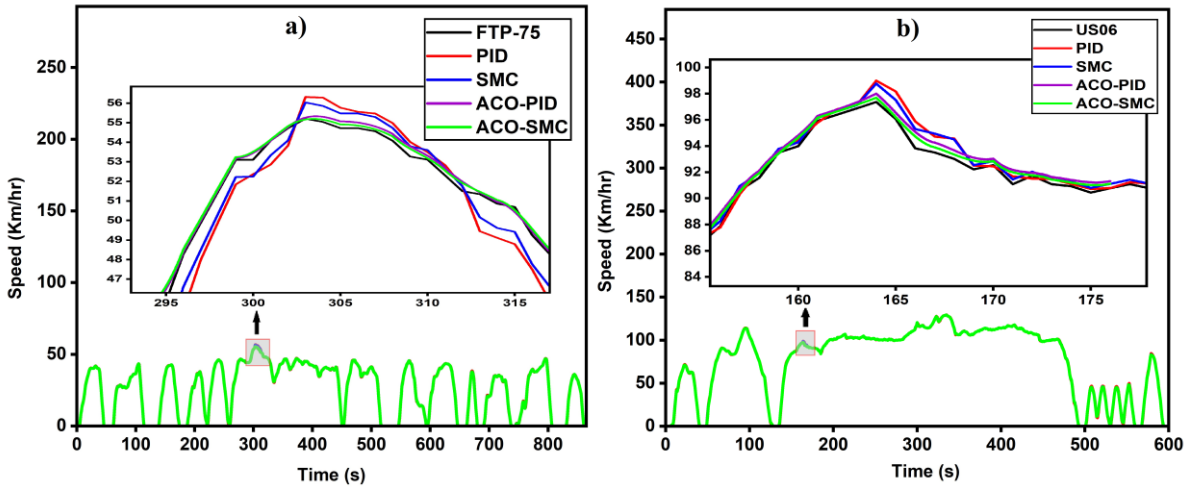

Figure 8. Performance of the controller under the influence of external disturbance for FTP-75 and US06

4.1.4. Sensitivity analysis

The robustness of the controllers is tested by varying key EV system parameters such as mass (m), drag coefficient (C_d), rolling resistance coefficient (μ_r), and EV tire radius (r). Figure 9 illustrates the robustness of the proposed controller under variations in EV system parameters, including a 20% increase in mass (m), 25% increase in tire radius (r), 20% decrease in drag coefficient(C_d), and a 30% increase in rolling resistance coefficient (μ_r). It is observed that the ACO-SMC controller completes full-power acceleration faster and stabilizes faster than the other controllers in the presence of uncertainties.

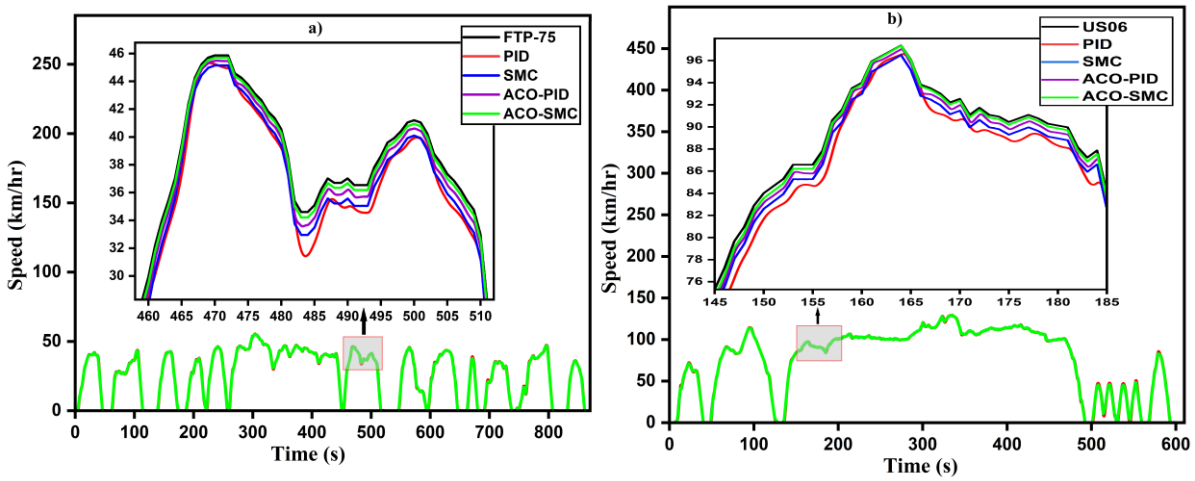

Figure 9. Robustness of the controller against the EV parameter variations for FTP-75 and US06

4.2. Frequency-Domain Analysis of ACO-SMC Controller

The sensitivity function represents the system's ability to achieve accurate set-point tracking, while the complementary sensitivity function indicates the robustness against external road disturbance noise. It is observed from Figure 10 that the sensitivity function must have

https://doi.org/10.31436/iiumej.v26i2.4136

smaller values at low frequencies, while the complementary sensitivity function in Figure 11 must have smaller values at higher frequencies.

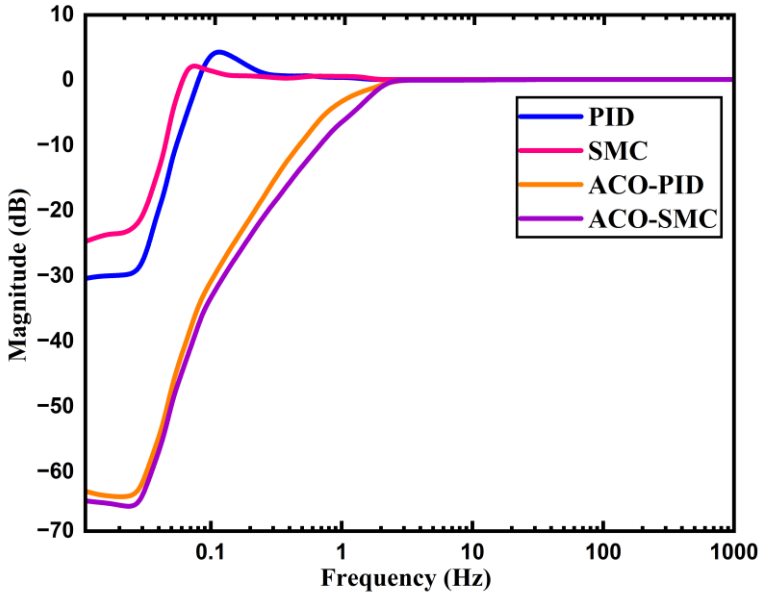

Figure 10. Frequency domain plots of the sensitivity function

The essential frequency-domain relationships for the sensitivity and complementary sensitivity functions can be expressed as follows:

$$S(s) = \frac{1}{1+L(s)} \tag{31}$$

$$T(s) = \frac{L(s)}{1+L(s)} \tag{32}$$

where, $L(s) = G(s)\,C(s)$ is the loop transfer function, $G(s)$ is the plant transfer function, and $C(s)$ is the controller transfer function.

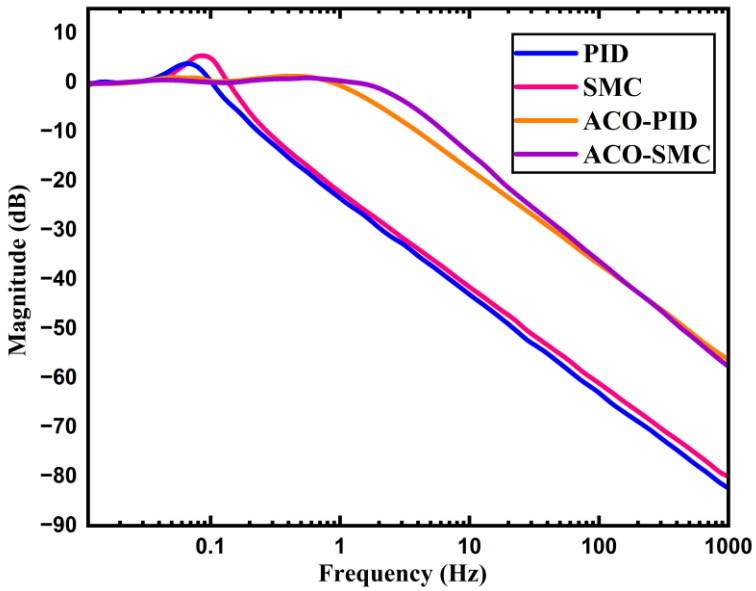

Figure 11. Frequency domain plots of the complementary sensitivity function

5. CONCLUSION

This study presented an improved ACO-SMC control strategy to enhance the speed control performance of an electric vehicle under standard driving cycles. The simulation results confirm that the proposed ACO-SMC controller achieved superior tracking performance, faster dynamic response, and significantly reduced tracking errors and chattering compared to PID, SMC, and ACO-PID controllers under both FTP-75 and US06 driving cycles. In addition, the proposed controller exhibits strong robustness against varying driving conditions, external disturbances, and system constraints, ensuring smooth and stable vehicle operation. However, this study is limited to simulation-based validation using a DC motor-driven electric vehicle model and does not include real-time experimental implementation. Furthermore, the inverter switching dynamics, thermal effects, and battery nonlinearities were not considered in detail. Future work will focus on the real-time implementation of the proposed controller on hardware platforms, extension to induction-motor-based electric vehicles, and experimental validation under practical operating conditions to further verify its effectiveness and applicability in real-world EV systems.

ACKNOWLEDGEMENT

The author would like to acknowledge the support, contribution, and sincere gratitude to the management of Vellore Institute of Technology, Vellore campus, Tamil Nadu, India.

REFERENCES

[1] Lee W J, Strbac G, Hu Z, Ding Z, Sarikprueck P, Teng F, and Kariniotakis G. (2020). Special issue on advanced approaches and applications for electric vehicle charging demand management. IEEE Transactions on Industry Applications 56(12): 5682–5683.

[2] Khooban M H, Niknam T, Blaabjerg F, and Dehghani M. (2016). Free chattering hybrid sliding mode control for a class of non-linear systems: electric vehicles as a case study. IET Science, Measurement & Technology 10(8): 776–785.

[3] Hermassi, M., Krim, S., Kraiem, Y., & Hajjaji, M. A. (2024). Adaptive neuro fuzzy technology to enhance PID performances within VCA for grid-connected wind system under nonlinear behaviors: FPGA hardware implementation. Computers and Electrical Engineering, 117, 109264.

[4] Arya Y. (2019). Impact of ultra-capacitor on automatic generation control of electric energy systems using an optimal FFOID controller. International Journal of Energy Research 43(14): 8765–8778.

[5] Patel V V. (2020). Ziegler–Nichols tuning method: understanding the PID controller. Resonance 25(12): 1385–1397.

[6] Hannan M A, Ali J A, Hossain Lipu M S, Mohamed A, Ker P J, Mahlia T M I, and Dong Z Y. (2020). Role of optimization algorithms based on fuzzy controllers in achieving induction motor performance enhancement. Nature Communications 11(1): 3792.

[7] Hou M, Zhao Y, and Ge X. (2017). Optimal scheduling of the plug-in electric vehicles aggregator energy and regulation services based on grid-to-vehicle. International Transactions on Electrical Energy Systems 27(12): e2364.

[8] Kashfi, R., Balochian, S., & Alishahi, M. (2024). Design of a optimal robust adaptive neural network-based fractional-order PID controller for H-bridge single-phase inverter. Applied Soft Computing, 166, 112142.

[9] Freitas, J. B. S., Marquezan, L., de Oliveira Evald, P. J. D., Peñaloza, E. A. G., & Cely, M. M. H. (2024). A fuzzy-based Predictive PID for DC motor speed control: JBS Freitas et al. International Journal of Dynamics and Control, 12(7), 2511-2521.

[10] Qu, S., Xu, W., Zhao, J., & Zhang, H. (2021). Design and implementation of a fast sliding-mode speed controller with disturbance compensation for SPMSM system. IEEE Transactions on Transportation Electrification, 7(4), 2611-2622.

[11] Chen, X., Zhao, J., Lu, Y., & Sheng, L. (2025). Research on sliding mode speed control method of permanent magnet drive system in shearer cutting section based on sliding mode observer under complex working conditions: X. Chen et al. International Journal of Dynamics and Control, 13(6), 234.

[12] Mousmi A, Abbou A, and El Houm Y. (2019). Real-time implementation of a novel hybrid fuzzy sliding mode control of a BLDC motor. International Journal of Power Electronics and Drive Systems 10(3): 1167–1177.

[13] Wu L, Liu J, Vazquez S, and Mazumder S K. (2021). Sliding mode control in power converters and drives: a review. IEEE/CAA Journal of Automatica Sinica 9(2): 392–406.

[14] Chan J W. (2022). Sliding mode control of brushless DC motor speed control. Malaysian Journal of Science and Advanced Technology 2(4): 188–193.

[15] Levant A. (2003). Higher-order sliding modes, differentiation, and output-feedback control. International Journal of Control 76(9): 924–941.

[16] Liu J, Zhao T, and Dian S. (2021). General type-2 fuzzy sliding mode control for motion balance adjusting of the power-line inspection robot. Soft Computing 25(2): 1033–1047.

[17] Flores Peña P, Luna M A, Ale Isaac M S, Ragab A R, Elmenshawy K, Martín Gómez D, and Molina M. (2022). A proposed system for multi-UAVs in remote sensing operations. Sensors 22(23): 9180.

[18] George M A, Kamat D V, and Kurian C P. (2021). Electronically tunable ACO-based fuzzy FOPID controller for effective speed control of an electric vehicle. IEEE Access 9(15): 73392–73412.

[19] Khooban M H, ShaSadeghi M, Niknam T, and Blaabjerg F. (2017). Analysis, control, and design of speed control of electric vehicles delayed model: multi-objective fuzzy fractional-order controller. IET Science, Measurement & Technology 11(2): 249–261.

[20] George, M. A., Kamat, D. V., & Kurian, C. P. (2024). Electric vehicle speed tracking control using an ANFIS-based fractional order PID controller. Journal of King Saud University-Engineering Sciences, 36(4), 256-264.

[21] Xu, M. (2022, November). Control of DC adjustable speed electric vehicle based on PSO-PID algorithm optimization research. In 2022 IEEE 5th International Conference on Automation, Electronics and Electrical Engineering (AUTEEE) (pp. 616-621). IEEE.